

REGULAR PAPER

## Estimation error in sound velocity depending on size of target scatterer

To cite this article: Aoi Nakayama *et al* 2021 *Jpn. J. Appl. Phys.* **60** SDDE17

View the [article online](#) for updates and enhancements.



## Estimation error in sound velocity depending on size of target scatterer

Aoi Nakayama<sup>1</sup>, Shohei Mori<sup>2\*</sup>, Mototaka Arakawa<sup>1,2</sup>, and Hiroshi Kanai<sup>1,2</sup>

<sup>1</sup>Graduate School of Biomedical Engineering, Tohoku University, Sendai, Miyagi 980-8579, Japan

<sup>2</sup>Graduate School of Engineering, Tohoku University, Sendai, Miyagi 980-8579, Japan

\*E-mail: [mori@ecei.tohoku.ac.jp](mailto:mori@ecei.tohoku.ac.jp)

Received December 7, 2020; revised February 18, 2021; accepted March 30, 2021; published online April 28, 2021

The quality of ultrasonic images can be improved by estimating the sound velocity accurately. Our previous study proposed a method to estimate the sound velocity based on the difference between the reception times of radiofrequency signals received by elements in an ultrasonic probe. Because the method assumed an ideal point scatterer as the target, the estimation error in the sound velocity increased with an increase in the target scatterer size. In the present study, the effect of the target scatterer size on the estimation method was examined, and the relationship between the size of the target scatterer and the estimation error in the sound velocity was quantified. Through simulations and basic experiments, it was confirmed that the estimation error was caused by the change in the reception time from the target surface and that the estimation error depended on the depth and size of the target scatterer. © 2021 The Japan Society of Applied Physics

### 1. Introduction

Medical ultrasound is useful in the diagnosis of diseases and the observation of various organs.<sup>1–3)</sup> Array probes are widely used in ultrasonic medical diagnosis, and the transmitting and receiving beams are formed by applying an appropriate delay time to each element of the probe,<sup>4,5)</sup> assuming that the sound velocity in vivo is  $1540 \text{ m s}^{-1}$ .<sup>6–9)</sup> However, the actual sound velocity in vivo depends on each tissue, therefore, the delay time cannot be corrected accurately. This difference in sound velocity deteriorates the image quality of the ultrasonic tomographic image.<sup>7,10,11)</sup> The average sound velocities in fat ( $1450 \text{ m s}^{-1}$ ) and muscle tissues ( $1647 \text{ m s}^{-1}$ ) are significantly different from those in other tissues ( $1540 \text{ m s}^{-1}$ ).<sup>12,13)</sup> Therefore, deterioration of the image quality is especially significant in the ultrasonic diagnosis of obese patients and breasts.<sup>14)</sup> This problem can be solved by estimating the sound velocity in vivo and reconstructing the received beam with an appropriate delay time.

Furthermore, it is expected that non-invasive diagnosis, such as the diagnosis of liver disease, will be realized by estimating the sound velocity in vivo. Recently, the number of patients with fatty liver has been increasing.<sup>15)</sup> It is known that there is a correlation between the fat content of the liver tissues and the tissue sound velocity.<sup>16–18)</sup> Therefore, if the sound velocity in the liver tissue can be estimated accurately, non-invasive and quantitative diagnosis of fatty liver<sup>19)</sup> is expected.

Many studies have been conducted to solve the problem of quality deterioration of ultrasonic tomographic images owing to the tissue dependence of the sound velocity in vivo. One of the methods is the phase aberration correction method,<sup>20,21)</sup> in which the delay set for each received beam is corrected by detecting the phase shift of the radiofrequency (RF) signals received by each element in the probe. While this method is advantageous for correcting the time delay error with high accuracy, it has the disadvantage of requiring a high computational capacity.<sup>19)</sup> In other methods,<sup>22–25)</sup> the focus quality factor (FQF) is calculated in the region of interest set in the measurement area. By changing the sound velocity used to form the received beams, the optimal sound velocity is determined such that the FQF is maximum. These methods require a significant computational load.

Methods for estimating not only the average sound velocity but also the local sound velocity distribution have been proposed.<sup>26–28)</sup> In the method proposed by Ali et al.,<sup>26)</sup> the average sound velocity was determined using the coherence factor (CF), and the local sound velocity was estimated using the average sound velocity. Sanno et al.<sup>27)</sup> developed a method to estimate the sound velocity distribution using the signal-to-noise ratio factor in addition to the CF. They demonstrated the effectiveness of each method through experiments with a wire phantom.

Our group has proposed a method to estimate the distribution of local sound velocity in each multi-layered medium based on the difference among the reception times of RF signals received by the elements in an ultrasonic probe.<sup>28)</sup> However, this method assumed the ideal point scatterer as the target. In a previous study, the estimation error in the sound velocity was always positive and increased as the diameter of the target scatterer became larger.<sup>29)</sup> In our previous study,<sup>29)</sup> the effect of the target scatterer size on the previously proposed sound velocity estimation method<sup>28)</sup> was confirmed by simulations and experiments. However, the relationship between the size of the target scatterer and the estimation error was not quantified.

In the present study, we quantified the estimation error influenced by the size of the target scatterer on the sound velocity estimation method<sup>28)</sup> by approximating that the first arrival wave from the surface of the target scatterer was dominant in the sound velocity estimation. From simulated and basic experiments, the relationship between the target scatterer size and the estimation error in the sound velocity was confirmed.

### 2. Principle and methods

#### 2.1. Previous estimation method of sound velocity assuming ideal point scatterer as target

We now briefly explain the sound velocity estimation method in a homogeneous medium using scattered waves from an ideal point scatterer. In the previously proposed method, the sound velocity was estimated in each of the multi-layered mediums.<sup>28)</sup> However, in the present study, the target medium is assumed to be homogeneous to concentrate the discussion on the effect of the size of the target scatterer. A target ideal point scatterer is set at a depth  $d$  below the central

element of the linear probe, as shown in Fig. 1(a). The wave scattered from the point scatterer is received by each element in the probe. We describe the propagation time,  $T_0(x_k)$ , as the total time during which a plane ultrasonic wave is transmitted from the probe, scattered by the ideal point scatterer at  $(0, d)$ , and received by the  $k$ th element at  $(x_k, 0)$ .  $T_0(x_k)$  is geometrically given by

$$T_0(x_k) = \frac{d + \sqrt{x_k^2 + d^2}}{c}, \quad (1)$$

where  $c$  is the sound velocity in the medium. The square  $\{T_0(x_k) - T_0(0)/2\}^2$  is described by the following quadratic function:

$$\left\{ T_0(x_k) - \frac{T_0(0)}{2} \right\}^2 = \frac{1}{c^2} x_k^2 + \frac{d^2}{c^2} = a x_k^2 + b, \quad (2)$$

where  $a$  and  $b$  are the coefficients of the quadratic function. From the quadratic approximation applied to the square of the measured propagation time  $\{t(x_k) - t(0)/2\}^2$ , the sound velocity  $c$  and the depth  $d$  are estimated as follows:

$$\hat{c} = \sqrt{\frac{1}{a}}, \quad (3)$$

$$\hat{d} = \sqrt{\frac{b}{a}}. \quad (4)$$

### 2.2. Effect of scatterer size on sound velocity estimation

The target scatterer has a finite size in vivo. We considered the effect of a finite-sized target scatterer with radius  $r$  on the estimated sound velocity using the aforementioned method. We assumed that the focused wave was approximated by a plane wave near the focal region, and only the scattered wave from within the focal region was received by the ultrasonic element. A schematic of the first arrival wave from the surface of a cylindrical scatterer with radius  $r$  is shown in Fig. 1(b). The blue straight lines show the propagation paths of the scattered waves, each of which is transmitted from the central element, scattered from the scatterer at point A  $(0, d)$ , and received by the central element or  $k$ th element. The red straight lines show the propagation paths of the waves scattered at the surface other than point A and received by the central element or  $k$ th element.

The RF wave received by the  $k$ th element is composed of scattered waves. When the target is an ideal point scatterer, that is,  $r$  is considerably smaller than the wavelength, the first arrival wave among the RF waves received by the  $k$ th element is shown by the blue path. However, when the target scatterer has a finite size, there is a first arrival wave other than the ones indicated by the blue path, for example, shown by the red path in Fig. 1(b), and the first arrival wave indicated by the red path is received earlier than that indicated by the blue path as  $r$  increases.

The curvature coefficient  $a$  of the quadratic function in Eq. (2) is determined by the difference between the arrival times to the elements. When the scatterer has a finite size,  $a$  becomes smaller than that of the ideal point scatterer, as shown by the dashed blue line in Fig. 1(b). Therefore, the sound velocity, estimated using Eq. (3), is higher than the

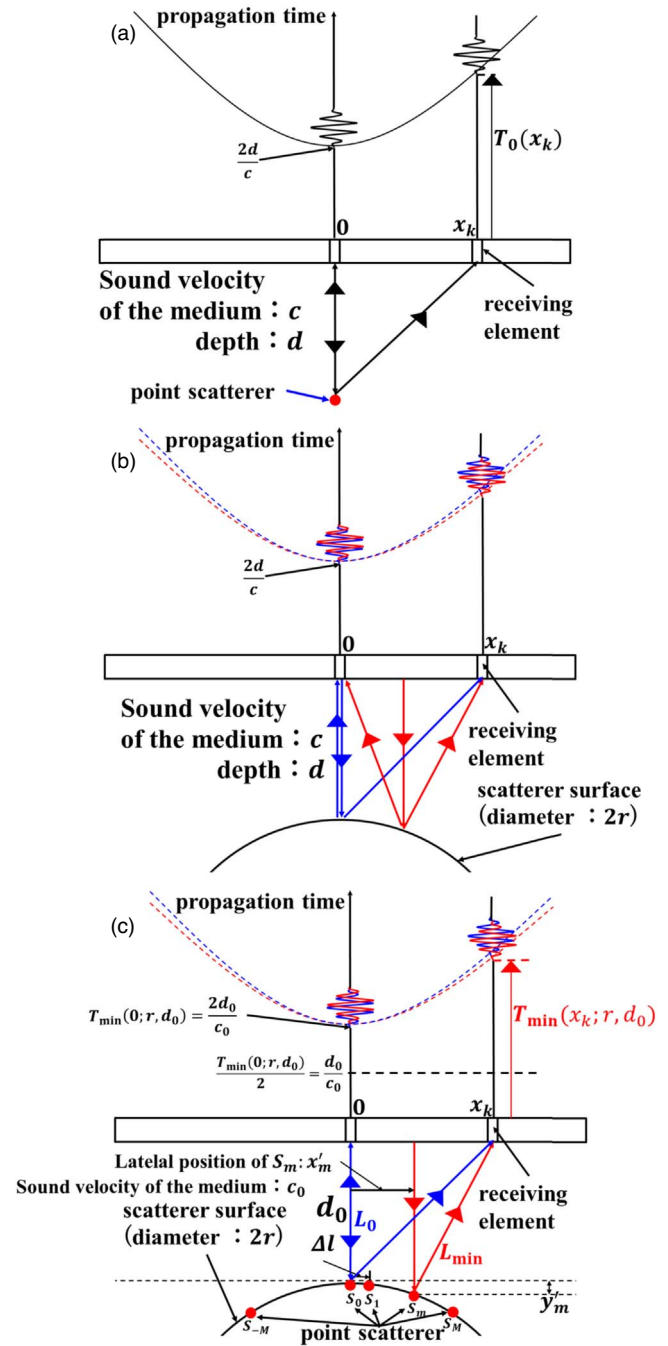


**Fig. 1.** (Color online) (a) Schematic of the reception of scattered waves from an ideal point scatterer.<sup>29)</sup> (b) Schematic of the reception of scattered waves from the surface of a scatterer with a finite size. (c) The simulation model in which multiple ideal point scatterers are on the scatterer surface.<sup>29)</sup>

true value as the scatterer size increases, and the estimation error increases positively.

### 2.3. Quantification of relationship between target scatterer size and error in sound velocity estimation

To quantify the estimation error described in the previous section, we consider the first arrival wave received by the  $k$ th element, as shown in Fig. 1(c). For this purpose, let us assume that the surface of the scatterer with a radius  $r$  is composed of many ideal point scatterers set on the surface of the scatterer at circumferential intervals  $\Delta l$ , as shown in Fig. 1(c).

The blue straight lines show the propagation paths of the wave transmitted from the central element, scattered at point

$S_0$ , and received by the central element or  $k$ th element. The blue dashed line shows the parabola of the propagation time distribution when the scatterer is an ideal point. The length of the path  $L_0(x_k)$  is geometrically expressed as

$$L_0(x_k) = d_0 + \sqrt{x_k^2 + d_0^2}. \quad (5)$$

Meanwhile, the red straight lines show the propagation path of the wave transmitted from the element above the point scatterer  $S_m$ , scattered at point  $S_m$ , and received by the  $k$ th element. The red dashed line shows the parabola of the propagation time distribution of the first arrival wave when the scatterer has a radius  $r$ . The length of the red path  $L(x_k, x'_m; r, d_0)$  is geometrically expressed as

$$L(x_k, x'_m; r, d_0) = d_0 + r - \sqrt{r^2 - x_m'^2} + \sqrt{(x_k - x'_m)^2 + (d_0 + r - \sqrt{r^2 - x_m'^2})^2}, \quad (6)$$

where  $x'_m$  is the lateral position of the  $m$ th ideal point scatterer  $S_m$  and is given by

$$x'_m = r \sin\left(\frac{m\Delta l}{r}\right). \quad (7)$$

The minimum of  $L_{\min}(x_k; r, d_0)$  is determined by

$$L_{\min}(x_k; r, d_0) = \min_{x'_m} L(x_k, x'_m; r, d_0). \quad (8)$$

We define the minimum propagation time of the red paths by  $T_{\min}(x_k; r, d_0)$ ,

$$T_{\min}(x_k; r, d_0) = \min_{x'_m} T(x_k, x'_m; r, d_0), \quad (9)$$

where  $T(x_k, x'_m; r, d_0)$  represents the propagation time of the red path in Fig. 1(c). The scatterer with  $r \approx 0$  is an ideal point scatterer. The square  $\{T_{\min}(x_k; r \approx 0, d_0) - T_0(0; r \approx 0, d_0)/2\}^2$  is approximated by

$$\left\{ T_{\min}(x_k; r \approx 0, d_0) - \frac{T_{\min}(0; r \approx 0, d_0)}{2} \right\}^2 \approx \left\{ T_0(x_k) - \frac{T_0(0)}{2} \right\}^2 = \frac{1}{c_0^2} x_k^2 + \frac{d_0^2}{c_0^2}, \quad (10)$$

where  $c_0$  is the true sound velocity in the medium. Equation (10) is equal to Eq. (2) in the case where  $c = c_0$ , and the sound velocity can be estimated using Eq. (3) as the target scatterer is an ideal point scatterer. For the scatterer with  $r \gg 0$ ,  $\{T_{\min}(x_k; r, d_0) - T_{\min}(0; r, d_0)/2\}^2$  does not coincide with Eq. (2).

From Eqs. (6)–(10), the relative estimation error  $Err(x_k; r, d_0)$  of the sound velocity is given by:

$$Err(x_k; r, d_0) \triangleq \frac{\hat{c} - c_0}{c_0} = \frac{\sqrt{x_k^2 + \hat{d}^2}}{r - \sqrt{r^2 - \{x_{m,\min}(x_k; r, d_0)\}^2} + \sqrt{(x_k - x_{m,\min}(x_k; r, d_0))^2 + (d_0 + r - \sqrt{r^2 - \{x_{m,\min}(x_k; r, d_0)\}^2})^2}} - 1, \quad (11)$$

where

$$x_{m,\min}(x_k; r, d_0) = \operatorname{argmin}_{x'_m} L(x_k, x'_m; r, d_0). \quad (12)$$

Equation (11) shows that the relative estimation error  $Err(x_k; r, d_0)$  does not depend on the true sound velocity  $c_0$ , and it is a function of the element position  $x_k$ , the radius of the scatterer  $r$ , and the depth of the scatterer  $d_0$ .

#### 2.4. Simulated experimental method

From the simulated experiment, the minimum value,  $t_{\min}(x_k; r, d_0)$ , of the propagation times of the first arrival waves that are transmitted from the position  $(x_k, 0)$ , scattered at the target scatterers, and received by the  $k$ th element, is quantitatively determined by

$$t_{\min}(x_k; r, d_0) = \frac{1}{c_0} L_{\min}(x_k; r, d_0). \quad (13)$$

The simulated experiment was conducted under the following conditions in the model shown in Fig. 1(c).  $\Delta l$  was set to 1  $\mu\text{m}$ . The true value of the sound velocity was set to 1495  $\text{m s}^{-1}$ . To simulate the wave scattered at the surface of the target scatterer, the experimentally measured waveform from a tungsten wire with a diameter of 0.03 mm in a water tank was received at the central element and used as the ultrasound pulse waveform  $h_0(t)$  scattered from the ideal point scatterer and received by the 0th element at the position  $(0, 0)$ .

The difference between the delay time of the scattered wave from the  $m$ th point scatterer  $S_m$  and that of the scattered wave from the 0th point scatterer  $S_0$ , received at the  $k$ th element, is determined by

$$\tau_{mk}(x_k, x'_m; r, d_0) = \frac{1}{c_0} \{L(x_k, x'_m; r, d_0) - L(0, 0; r, d_0)\}. \quad (14)$$

The received waveform at the  $k$ th element, composed of the scattered waves from multiple positions on the scatterer surface, is obtained by

$$h_k(t; x_k, r, d_0) = \sum_{m=-M}^M h\{t - \tau_{mk}(x_k, x'_m; r, d_0)\}. \quad (15)$$

The ultrasonic propagation time  $t(x_k; r, d_0)$  is determined by detecting the peak of the simulated waveform  $h_k(t; x_k, r, d_0)$  at the  $k$ th element. By approximating each of the resultant distributions  $\{t_{\min}(x_k; r, d_0)\}$  and  $\{t(x_k; r, d_0)\}$  by the quadrature function, the sound velocity is estimated using Eq. (3).

#### 2.5. Experimental method

Using wires of different sizes as the target scatterers, the effect of the target scatterer size on the sound velocity estimation was confirmed through a basic experiment. In

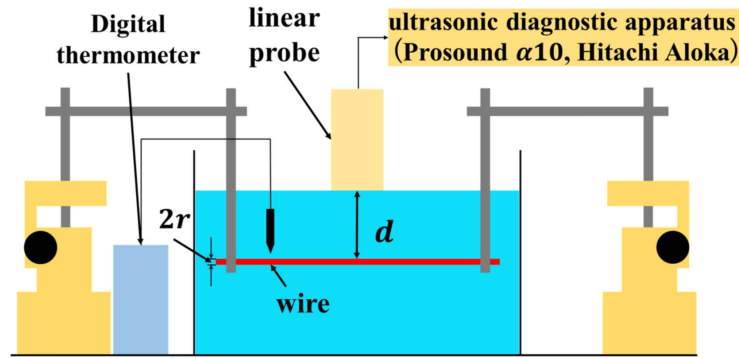


Fig. 2. (Color online) Experimental configuration.

the simulated experiment, the focused wave was approximated by a plane wave near the focal region; however, the focused wave was transmitted in this basic experiment using wires. The experimental setup is illustrated in Fig. 2. Ultrasonic diagnostic equipment (Prosound α10, Hitachi Aloka, Japan) was used with a linear probe (UST-5412, Hitachi Aloka, Japan). The transmission frequency was set at 7.5 MHz, the sampling frequency was set at 40 MHz, and 96 elements were used for transmitting and receiving ultrasonic beams.

A tungsten wire with a diameter of 0.03 mm, nylon wires with diameters of 0.25, 0.50, 0.75, and 0.90 mm, and silicone rubber wires with diameters of 2.0, 3.0, 4.0, 5.0, and 6.0 mm were used as the target scatterers. The top surface of each wire was set at a depth of 30 mm from the probe surface in the water. The RF signals were acquired 10 times by rearranging the position of the wire for each measurement. The focal point was also set to a depth of 30 mm.

The depth dependence of the relative estimation error was investigated using a similar basic experiment by changing the target depth. Several wires with diameters of 0.03, 0.50, 0.90, 3.0, and 6.0 mm were used as the target scatterers. The top surface of each wire was set at a depth of 40 mm from the probe surface in the water. The focal point was set to a depth of 40 mm. Other conditions were the same as in the basic experiment when the depth was set at a depth of 30 mm from the probe surface in the water.

### 3. Results and discussion

#### 3.1. Determination of propagation time in basic experiment

The ultrasonic propagation time  $t(x_k)$  was determined by detecting the positive peak of the received waveform at each receiving element. The detected  $n$ th positive peak time  $t_{\text{peak}}(x_k)$  of the waveform was corrected to the rise time  $t(x_k)$  of the pulse wave as follows:

$$t(x_k) = t_{\text{peak}}(x_k) - \frac{n - 0.75}{f_0}, \quad (16)$$

where  $f_0$  is the transmission frequency. Figure 3(a) shows the waveform of the scattered wave from the scatterer received by the central element in the case of the scatterer with a diameter of 0.25 mm. Figure 3(b) shows the waveforms  $h(t)$  and  $h(t - \tau_{\text{AP}})$ , which simulated the scattered waves from the anterior and posterior walls of the scatterer, respectively, where  $\tau_{\text{AP}}$  is the delay in the reception time of the scattered waves from the posterior wall concerning that of the scattered

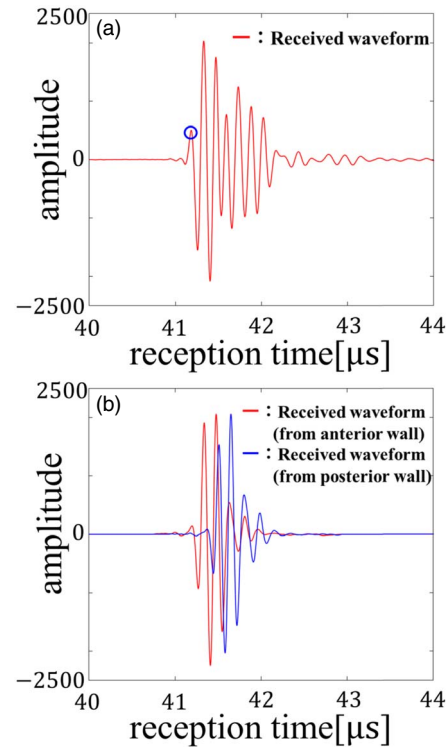


Fig. 3. (Color online) Received waveform at the central element (0.25 mm) (a) measured in the basic experiment and (b) generated by the simulated experiment (red line: from the anterior wall, blue line: from the posterior wall).<sup>29)</sup>

waves from the anterior wall. By comparing the waveforms in Figs. 3(a) and 3(b), it was observed that the scattered waves from both the walls interfered.

Therefore, to suppress the interference, the position of the peak (O) in Fig. 3(a) was determined for the scattered waves from the anterior wall for a diameter of  $2r \geq 0.25$  mm. For a diameter of  $2r = 0.03$  mm, however, the delay time between the scattered waves from the anterior and posterior walls was approximately only a 0.1 period of the transmitted wave. Therefore, the scattered waves from the anterior and posterior walls could not be separated. Thus, the position of the peak was determined for the interfered waveform of the wire. The effect of the interference of the scattered waves on the determination of the propagation time for the thin wire should be examined in the future.

#### 3.2. Propagation time for ideal point scatterer and larger scatterers

Figure 4 shows the propagation time distributions determined using Eq. (14) when the scatterer is an ideal point scatterer

with a diameter of  $2r \approx 0$  and when the diameter  $2r$  is 6.0 mm. From Fig. 4, it was observed that the coefficient  $a$  of the parabola of the propagation time distribution became small when the diameter was 6.0 mm, which corresponded to the cause of the increase in the estimation error of the sound velocity described in Sect. 2.2.

### 3.3. Estimated sound velocities

Figure 5 shows the sound velocities estimated in the simulated experiments and the basic experiments using wires. The true sound velocity  $c_0$  was determined from the temperature of the water.<sup>30)</sup> Since the water temperature was different in each measurement, the true sound velocities were determined as  $1495 \text{ m s}^{-1}$  (for  $2r = 0.90\text{--}6.0 \text{ mm}$ ),  $1496 \text{ m s}^{-1}$  (for  $2r = 0.50, 0.75 \text{ mm}$ ), and  $1497 \text{ m s}^{-1}$  (for  $2r = 0.03, 0.25 \text{ mm}$ ). The averages and standard deviations of the estimated sound velocities in 10 measurements are shown by red dots and error bars, respectively.

The estimation error in the sound velocity increased with the diameter of the scatterer for both basic and simulated experiments. The results from the simulated and basic experiments were within 0.3%. From these results, it was confirmed that the increase in the sound velocity estimation error, because of the increase in the diameter of the scatterer, was caused by the first arrival wave from the surface of the scatterer.

### 3.4. Relationship between size of target scatterer and estimation error in sound velocity

Figure 6 shows the relative estimation error  $Err(x_k; r, d_0)$  of the sound velocity calculated using Eq. (11), and the measured estimation error ratio  $(\hat{c} - c_0)/c_0$  for the experimental results in Fig. 5. The averages and standard deviations of the estimated sound velocities for the 10 measurements are indicated by red dots and error bars, respectively. For  $Err(x_k; r, d_0)$ , the results  $\{Err(x_k; r, d_0)\}$  for various  $\{x_k\}$  values were averaged over  $x_k$ , and the average value is shown by the solid line.

The relative estimation error  $\{Err(x_k; r, d_0)\}$  corresponded well with the measured estimation error ratio  $(\hat{c}_{\text{sim}} - c_0)/c_0$  in the simulated results considering the first arrival wave, and the difference between  $\{Err(x_k; r, d_0)\}$  and  $(\hat{c}_{\text{sim}} - c_0)/c_0$  was within 0.024%. However, in the basic experiment, the measured estimation error  $(\hat{c}_{\text{exp}} - c_0)/c_0$  did not match well with the averaged value  $\{Err(x_k; r, d_0)\}$ , and the difference

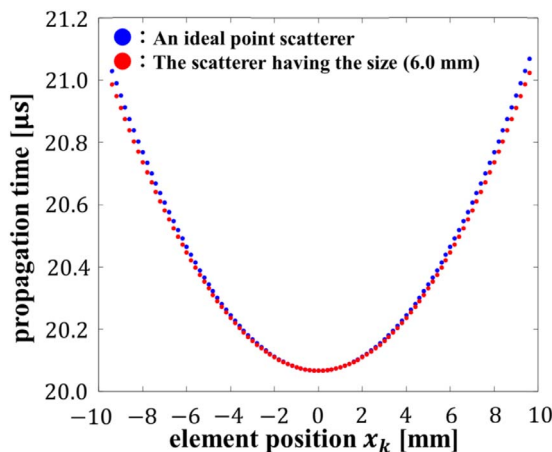


Fig. 4. (Color online) The propagation time distributions for the ideal point scatterer (blue) and the scatterer with a size (red) in the simulated experiment.

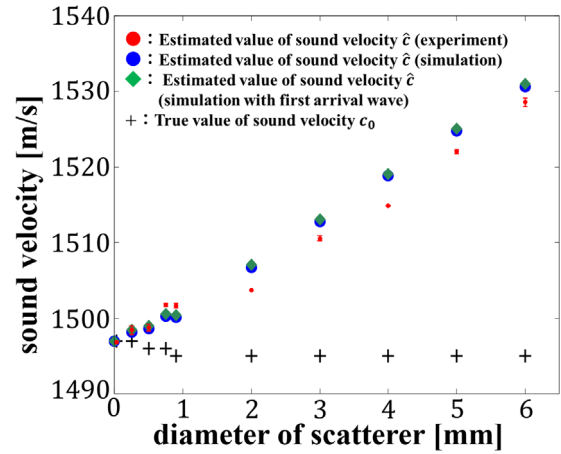


Fig. 5. (Color online) Estimated results of the sound velocity in the simulated experiment and the basic experiment using wires. The red dots and the error bars show the average values and the standard deviations of the estimated sound velocities in the basic experiments, respectively; the blue dots show the estimated sound velocities in the simulations with the interference waveform; the diamond symbols show the estimated sound velocities in the simulations with the first arrival wave, and black “+” symbols show the true values of the sound velocity.

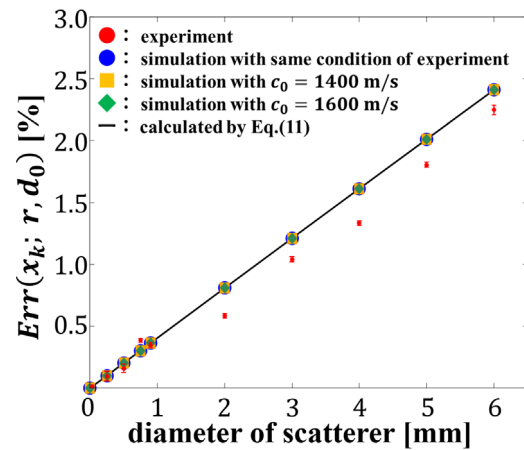
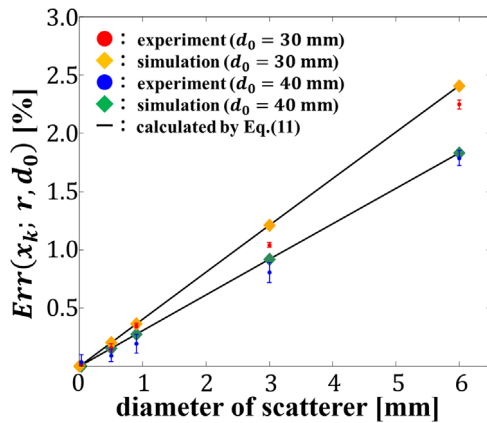


Fig. 6. (Color online) Estimation error ratio of the sound velocity. The red dots and the error bars show the average values and the standard deviations of the estimation error ratios in the basic experiment, respectively; the blue dots show the estimation error ratios in the simulations with the same condition of the experiment, rectangle symbols show the estimation error ratios in simulations with  $c_0 = 1400 \text{ m s}^{-1}$ , the diamond symbols show estimation error ratios in simulations with  $c_0 = 1600 \text{ m s}^{-1}$ , and the straight line represents the estimation error ratios calculated by Eq. (11).

between  $\{Err(x_k; r, d_0)\}$  and  $(\hat{c}_{\text{exp}} - c_0)/c_0$  was within 0.31%. From the results, it was confirmed that the relative estimation error depends on not the true sound velocity but the radius of the target scatterer at a certain depth.

Figure 7 shows the relative estimation errors  $Err(x_k; r, d_0)$  of the sound velocity when the depths of the scatterer were set to  $d_0 = 30 \text{ mm}$  and  $40 \text{ mm}$ . When the target depth  $d_0$  was  $40 \text{ mm}$ , the relative estimation error  $\{Err(x_k; r, d_0)\}$  corresponded well with the measured estimation error ratio  $(\hat{c}_{\text{sim}} - c_0)/c_0$  in the simulated results considering the first arrival wave, although the difference between  $\{Err(x_k; r, d_0 = 40 \text{ mm})\}$  and  $(\hat{c}_{\text{exp}} - c_0)/c_0$  was within 0.21%. The relative estimation error  $Err(x_k; r, d_0 = 40 \text{ mm})$  of the sound velocity was different from  $Err(x_k; r, d_0 = 30 \text{ mm})$ . These results confirmed the depth



**Fig. 7.** (Color online) Estimation error ratio of sound velocity at different depths ( $d_0 = 30$  and  $40$  mm). The red dots and the error bars show the average values and the standard deviations of the estimation error ratios in the basic experiments ( $d_0 = 30$  mm), respectively, the orange diamond symbols show the estimation error ratios in simulations ( $d_0 = 30$  mm), the blue dots and error bars show the average value and the standard deviations of the estimation error ratios in the basic experiments ( $d_0 = 40$  mm), respectively; the green diamond symbols show the estimation error ratios in the simulations ( $d_0 = 40$  mm), and the straight-lines represent the estimation error ratios calculated by Eq. (11).

dependence of the relative estimation error  $Err(x_k; r, d_0)$  of the sound velocity.

From these results, it was confirmed that the relative estimation error of sound velocity  $Err(x_k; r, d_0)$  can be quantified as a function of the depth and radius of the target scatterer. However, the relative estimation error  $Err(x_k; r, d_0)$  in the basic experiment was lower than that in the simulated experiment and that calculated using Eq. (11) for scatterers with diameters greater than 2 mm. It is a future task to clarify the cause of this difference.

#### 4. Conclusions

In the present study, we quantified the effect of the size of the scatterer on the sound velocity estimation method. To investigate the effect, we considered a model in which multiple ideal point scatterers were lined up on the surface of the scatterer, and conducted experiments simulating a situation in which ultrasonic waves were scattered on the surface. We also conducted a basic experiment using wires. It was confirmed that the relative estimation error of the sound velocity does not depend on the true value of the sound velocity, and this estimation error ratio can be quantified as a function of the depth and radius of the target scatterer. The results of the present study will lead to the proposal of an estimation method for sound velocity considering the effect of the target scatterer size in the future.

#### Acknowledgments

This work was partially supported by JSPS KAKENHI, Grant No. 20H02156.

- 1) J. A. Jensen, *Prog. Biophys. Mol. Biol.* **93**, 153 (2007).
- 2) M. Tanaka, T. Sakamoto, S. Sugawara, H. Nakajima, Y. Katahira, S. Ohtsuki, and H. Kanai, *J. Cardiol.* **52**, 86 (2008).
- 3) H. Kanai, M. Sato, Y. Koiwa, and N. Chubachi, *IEEE Trans. Ultrason. Ferroelectr. Freq. Control* **43**, 791 (1996).
- 4) J. F. Synnevag, A. Austeng, and S. Holm, *IEEE Trans. Ultrason. Ferroelectr. Freq. Control* **54**, 1606 (2007).
- 5) K. E. Thomenius, *IEEE Int. Ultrason. Symp.* **2**, 1615 (1996).
- 6) H.-C. Shin, R. Prager, H. Gomersall, N. Kingsbury, G. Treece, and A. Gee, *Ultrasound Med. Biol.* **36**, 623 (2010).
- 7) M. E. Anderson, M. S. McKeag, and G. E. Trahey, *J. Acoust. Soc. Am.* **107**, 3540 (2000).
- 8) M. Gyöngy and S. Kollár, *Ultrasonics* **56**, 370 (2015).
- 9) D. Fontanarosa, S. V. D. Meer, E. Harris, and F. Verhaegen, *Med. Phys.* **38**, 2665 (2011).
- 10) S. A. Goss, R. L. Johnston, and F. Dunn, *J. Acoust. Soc. Am.* **64**, 423 (1978).
- 11) S. A. Goss, R. L. Johnston, and F. Dunn, *J. Acoust. Soc. Am.* **68**, 93 (1980).
- 12) K. K. Shung, *Diagnostic Ultrasound: Imaging and Blood Flow Measurements*. (Taylor and Francis, Boca Raton, FL, 2005), p. 14.
- 13) A. Benjamin, R. E. Zubajlo, M. Dhyani, A. E. Samir, K. E. Thomenius, J. R. Grajo, and B. W. Anthony, *Ultrasound Med. Biol.* **44**, 2739 (2018).
- 14) F. Tranquart, N. Grenier, V. Eder, and L. Pourcelot, *Ultrasound Med. Biol.* **25**, 889 (1999).
- 15) M. Imbault, A. Faccineto, B.-F. Osmanski, A. Tissier, T. Deffieux, J.-L. Gennisson, V. Vilgrain, and M. Tanter, *Phys. Med. Biol.* **62**, 3582 (2017).
- 16) H. Hachiya, S. Ohtsuki, and M. Tanaka, *Jpn. J. Appl. Phys.* **33**, 3130 (1994).
- 17) H. Kumagai, K. Yokoyama, K. Katsuyama, S. Hara, H. Yamamoto, T. Yamagata, N. Taniguchi, N. Hirota, and K. Itoh, *Ultrasound Med. Biol.* **40**, 2499 (2014).
- 18) T. Yamaguchi, K. Inoue, J. Mamou, K. Kobayashi, and Y. Saijo, *Proc. Mtgs. Acoust.* **19**, 075011 (2013).
- 19) B. Boozari et al., *J. Ultrasound Med.* **29**, 1581 (2010).
- 20) D. Monjazebi and Y. Xu, *IEEE Int. Ultrason. Symp.*, 2019.
- 21) S. W. Flax and M. O'Donnell, *IEEE Trans. Ultrason. Ferroelectr. Freq. Control* **35**, 758 (1988).
- 22) C. Yoon, H. Seo, Y. Lee, Y. Yoo, T.-K. Song, and J. H. Chang, *IEEE Trans. Ultrason. Ferroelectr. Freq. Control* **59**, 905 (2012).
- 23) D. Napolitano, C.-H. Chou, G. McLaughlin, T.-L. Ji, L. Mo, D. DeBusschere, and R. Steins, *Ultrasonics* **44**, e43 (2006).
- 24) C. Yoon, Y. Lee, J. H. Chang, T.-K. Song, and Y. Yoo, *Ultrasonics* **51**, 795 (2011).
- 25) C.-C. Shen and H.-C. Yang, *Ultrasonics* **79**, 52 (2017).
- 26) R. Ali and J. J. Dahl, *IEEE Int. Ultrason. Symp.* 2019.
- 27) F. Sannou, R. Nagaoka, and H. Hasegawa, *Jpn. J. Appl. Phys.* **59**, SKKE14 (2020).
- 28) K. Abe, M. Arakawa, and H. Kanai, *J. Med. Ultrason.* **46**, 27 (2019).
- 29) A. Nakayama, S. Mori, M. Arakawa, and H. Kanai, *Proc. Symp. Ultrason. Electr.* **41**, 3Pa5-5 (2020).
- 30) W. Kroebl and K.-H. Mahrt, *Acta Acustica United Acustica* **35**, 154 (1976).